Storm Time Data Assimilation in the Thermosphere Ionosphere with TIDA

Mihail V. Codrescu[1], Stefan M Codrescu[2], and Mariangel Fedrizzi[3]

[1]NOAA-Space Weather Prediction Center
[2]Vector Space, LLC
[3]University of Colorado/CIRES and NOAA/SWPC

November 23, 2022

Abstract

Data assimilation schemes with empirical background models of the ionosphere are already in operational use. However such methods suffer during disturbed conditions when large gradients are present and are moving relatively fast through the modeled domain. Also, such schemes have limited forecasting capabilities. In order to improve disturbed conditions modeling, more sophisticated assimilation schemes based on sparse measurements for the coupled thermosphere ionosphere system are needed. We have implemented an ensemble Kalman Filter (enKF) for the Thermosphere-Ionosphere (TI) system. We used the Coupled Thermosphere Ionosphere Plasmasphere electrodynamics (CTIPe) model as the background for an assimilation scheme and created the Thermosphere Ionosphere Data Assimilation (TIDA) software package. We published our first paper discussing neutral mass density assimilation during quiet geomagnetic conditions in Space Weather in 2018. In this paper we present results from experiments during the 2003 Halloween Storm, 27-31 October 2003, under very disturbed (K$_p$ = 9) conditions while assimilating GRACE-A and B, and CHAMP neutral density measurements. TIDA was able to simulate this disturbed period without using the L1 solar wind measurements which were contaminated by solar energetic protons, by estimating the model inputs from the density measurements. TIDA is being prepared to offer specification and short term forecasts of neutral density for satellite drag and debris collision avoidance for space traffic management. We also plan to offer long term (solar cycle length), average neutral density estimation for satellite fleet management.

Posted on 23 Nov 2022 — CC-BY-NC 4 — https://doi.org/10.1002/essoar.10505945.1 — This a preprint and has not been peer reviewed. Data may be preliminary.

Storm Time Data Assimilation in the Thermosphere Ionosphere with TIDA

M. V. Codrescu[1], S. M. Codrescu[2], and M. Fedrizzi[3]

[1]Space Weather Prediction Center, Boulder, CO 80305
[2]Vector Space LLC, Boulder, CO 80305
[3]CIRES University of Colorado and Space Weather Prediction Center, Boulder, CO 80305

Key Points:

- This study demonstrates the data assimilation potential improvement for the TI system modeling during severe geomagnetic storms
- The estimation of the neutral density covariance matrix with a 75 member ensemble of CTIPe runs does not require covariance localization
- TIDA can produce neutral density model results even in the absence of L1 system forcing measurements

Corresponding author: Mihail Codrescu, `Mihail.Codrescu@noaa.gov`

Abstract

Data assimilation schemes with empirical background models of the ionosphere are already in operational use. However such methods suffer during disturbed conditions when large gradients are present and are moving relatively fast through the modeled domain. Also, such schemes have limited forecasting capabilities. In order to improve disturbed conditions modeling, more sophisticated assimilation schemes based on sparse measurements for the coupled thermosphere ionosphere system are needed. We have implemented an ensemble Kalman Filter (enKF) for the Thermosphere-Ionosphere (TI) system. We used the Coupled Thermosphere Ionosphere Plasmasphere electrodynamics (CTIPe) model as the background for an assimilation scheme and created the Thermosphere Ionosphere Data Assimilation (TIDA) software package. We published our first paper discussing neutral mass density assimilation during quiet geomagnetic conditions in Space Weather in 2018. In this paper we present results from experiments during the 2003 Halloween Storm, 27-31 October 2003, under very disturbed ($K_p = 9$) conditions while assimilating GRACE-A and B, and CHAMP neutral density measurements. TIDA was able to simulate this disturbed period without using the L1 solar wind measurements which were contaminated by solar energetic protons, by estimating the model inputs from the density measurements. TIDA is being prepared to offer specification and short term forecasts of neutral density for satellite drag and debris collision avoidance for space traffic management. We also plan to offer long term (solar cycle length), average neutral density estimation for satellite fleet management.

Plain Language Summary

Data assimilation schemes with empirical background models are already in operational use. Here we present an assimilation scheme using an ensemble Kalman filter with a physics based numerical background model. We show simulations for October 27 - 31, 2003, a period that includes several large geomagnetic disturbances known as the Halloween storms. This assimilation exercise is in preparation for testing future neutral density data products.

1 Introduction

Tools for ensemble modeling and data assimilation in the terrestrial weather and ocean science have been developed (Hoar et al., 2009) and are in operational use. The use of an enKF in space weather is also not new. M. V. Codrescu et al. (2004) published a paper for neutral composition enKF assimilation in 2004. Although neutral composition was recognized to be one of the most important factors in ionospheric simulations during storms (Chartier et al., 2013), the lack of neutral composition measurements has prevented the operational implementation of enKFs in space weather products and services. However the importance of enKF for space weather research has been recognized, enKFs have been used in research, and papers have been published (Solomentsev et al., 2012; Morozov et al., 2013; Hsu et al., 2014; Chartier et al., 2016), and references therein.

Today, other kinds of assimilation models based on Gauss Markov (GM) Kalman Filter (KF) processes are more popular in operational settings (Spencer et al., 2004; Schunk et al., 2004; T. Fuller-Rowell et al., 2006; Jee et al., 2010; Jakowski et al., 2011; Borries et al., 2015). GM KF assimilation schemes are based on stationary predefined covariance matrixes that work best if large amounts of data are available to overwhelm the empirical background model. The sudden availability of large amounts of Total Electron Content (TEC) measurements from Global Navigation Satellite Systems (GNSS) signals made the ionosphere GM KF assimilation schemes feasible to implement. GM KF based assimilation schemes can be very good at ionosphere specification for past events, especially during quiet or moderately disturbed geomagnetic conditions when large amounts of data are available. However, in real-time environments they can suffer from data starvation and do not have forecasting capabilities beyond persistence with a predefined evolution toward climatology.

During disturbed conditions, GM KF schemes have difficulty because their predefined, quiet-time covariance matrixes do not keep pace with the changing system. To obtain the appropriate covariance matrix during disturbed conditions it would be necessary to perform variational analysis (Rockafellar & Wets, 1998) during every assimilation time step. However, for assimilation schemes with hundreds of thousands to millions of state elements, performing variational analysis every assimilation time step (15 - 30 minutes) is not practical and the covariance matrix needs to be estimated in some other way. An estimation of the covariance matrix using Monte Carlo methods was first proposed by Evensen (1994) as the ensemble Kalman Filter (enKF).

In a previous paper (S. M. Codrescu et al., 2018), we discussed assimilation results for total mass density and showed that assimilating measurements from one satellite improves the model results globally, during quiet conditions. In this paper, in Section 2, we discuss the dominant processes that make the TI covariance matrix non-stationary during disturbed geomagnetic conditions. The paper continues with an experiment using TIDA to assimilate GRACE-A, GRACE-B, and CHAMP neutral density measurements during the extreme geomagnetic 2003 Halloween storms. Section 3 gives an overview of the TIDA software and setup of the experiment. The measurement sources are described in Section 4, results presented in Section 5, and finally we conclude in Section 6.

2 The Thermosphere Ionosphere System

The global neutral density and composition of the thermosphere depend on system forcing and the interaction with the ionosphere (FullerRowell et al., 1994). The global electron and ion density structure, roughly from 50 to 1000 km altitude, are at any given time the result of a dynamic equilibrium between plasma production, loss, and transport, processes controlled to a large extent by neutral composition and neutral winds (T. J. Fuller-Rowell et al., 1997). The processes that affect neutral composition, density, and winds and the production, loss, and transport of plasma are highly variable on timescales of minutes to years and their relative importance can change as a function of location on the globe, Universal Time, storm commencement time, season, solar cycle, waves propagating from below, and the previous state of the ionosphere-thermosphere-magnetosphere system (Sarris, 2019). On short time-scales, the variations are controlled by a set of external energy inputs that include solar radiation absorption at a variety of wave lengths, solar energetic proton deposition, solar wind energy transfer through the magnetosphere that depends on the density and speed of the solar wind and the magnitude and orientation of the interplanetary magnetic field (IMF) (M. V. Codrescu et al., 2012), and waves propagating from below (Heelis & Maute, 2020). The influence of waves propagating from below will not be discussed further in this paper as their amplitudes and phases change slowly relative to the duration of a geomagnetic storm and their influence can be taken into account by an appropriate lower boundary condition in the assimilation background model.

2.1 The system During Quiet Geomagnetic Conditions

While the Thermosphere Ionosphere (TI) is never in a true steady state, it can reach quasi-steady state conditions if the system inputs are quasi-constant over some period of time (days), as it happens during prolonged quiet geomagnetic conditions (M. V. Codrescu et al., 2008). Under steady state conditions the system energy input is balanced by cooling through CO_2 and NO infrared emissions and diurnally reproducible patterns can be observed in most system state variables.

While in prolonged quiet periods, the TI system reaches a quasi-steady state that can last many days (Roble, 1992). The state is said to be in a diurnally reproducible pattern. Under such conditions statistical models of high-latitude convection electric fields (Weimer, 2005), particle precipitation (T. J. Fuller-Rowell & Evans, 1987), and solar EUV fluxes based on correlation with the F10.7 measurements (Hinteregger et al., 1981) are good enough to give acceptable model results when used in physics based numerical models of the system. In addition, empirical, statistical models of the ionosphere (Bilitza, 2018; Nava et al., 2008) or thermosphere climatology (Picone et al., 2002) are also good during quasi-steady state conditions. This means that during quiet conditions the system can be modeled with a high level of confidence.

During quasi-steady state conditions, a global equilibrium is established between heating due to solar radiation absorption on the dayside, Joule Heating at high latitudes and infrared cooling due to NO and CO_2. As a consequence, a diurnally reproducible global neutral temperature structure and circulation are established and a relatively stable global neutral composition structure is maintained (Killeen et al., 1997). This state of the thermosphere produces a diurnally reproducible global dynamo electric field pattern (Richmond, 1989) which in association with the stable prompt penetration electric field pattern of magnetospheric origin (Manoj & Maus, 2012) produce a diurnally reproducible ionosphere. During geomagnetically quiet conditions the energy input from solar radiation absorption dominates the system energy input (Mlynczak et al., 2016).

In the upper atmosphere around 300 km altitude where the peak electron density normally occurs, the temperature structure establishes day-night pressure gradients that drive the global circulation neutral winds (Hedin et al., 1991). The winds blow from the dayside towards the nightside, both east and west and over the poles from the 14:00 local time sector. Mostly molecular species are present below 150 km altitude and atomic species above. The difference between the Earth geographic and magnetic poles contributes to the diurnal variation in the global temperature, winds, and composition structure both in the sun-fixed reference frame and at any location on the globe.

2.2 The system During Disturbed Geomagnetic Conditions

During geomagnetic storms, changes in external system forcing cause large increases in the magnitude and distribution of Joule heating, in auroral particle precipitation total energy and its distribution, and in momentum transfer to neutrals. The total energy input into the TI system at high-latitudes increases dramatically and can become larger than solar radiation heating. This has dramatic consequences for the global neutral winds and composition. Furthermore, changes in neutral winds cause changes in the dynamo electric field pattern. Due to the tight coupling between the ionosphere and thermosphere the changes are then reflected in the ionosphere and feed-back to the neutral state through ion drag, momentum transfer, heat transfer, and other mechanisms (FullerRowell et al., 1994, 1996).

Empirical models are not appropriate to represent the state of the TI system during severe geomagnetic storms. Numerical models of the system also suffer during disturbed conditions because the statistical models used for forcing have very large uncertainties and this results in unacceptable uncertainties in model simulation results. Although disturbed conditions may happen only during a small percentage of time, it is during disturbed conditions that accurate modeling is most important.

Storm Joule heating occurs at high-latitudes at about 110-115 km altitude where molecular species (O_2 and N_2) dominate. The additional heating changes the pressure gradients and drives a storm circulation, in addition to the quiet time winds. Strong vertical winds are driven above the auroral zone heating area and meridional winds away from the heating area at higher altitudes. Vertical winds will take molecular species up and change the neutral composition creating what is called the composition bulge. Meridional winds will spread the bulge towards lower latitudes (Proelss & von Zahn, 1978).

During small disturbances the storm induced meridional winds are overwhelmed by the quiet time circulation on the dayside but add to it on the nightside resulting in a distortion of the composition bulge relative to the shape of the auroral zone. During large storms meridional winds can turn equatorward at mid-latitudes even on the dayside. The size, shape, and position of the auroral zone and the composition bulge are highly variable functions of solar wind density and speed, magnitude and orientation of the interplanetary magnetic field, and storm time.

During a geomagnetic storm molecular species are transported up (upwelling) above 200 km where they displace lighter atomic species (mostly atomic Oxygen). The lighter species are then forced equatorward by storm meridional winds. To balance the pressure gradients and close the storm circulation the lighter species are transported down (downwelling) by storm vertical winds at some distance equatorward of the heating area and a return poleward flow of molecular species takes place at lower altitudes (FullerRowell et al., 1994, 1996). The position of the upwelling area can vary in time but depends mostly on the intensity of the storm while the position of the downwelling area is a more complicated function of storm intensity, duration, and storm time profile.

The changes in neutral dynamics and composition cause important changes in the TI system (Proelss & von Zahn, 1978; FullerRowell et al., 1994; Burns et al., 1995; Fuller-Rowell et al., 1996). In the composition bulge, plasma production decreases due to the decreased atomic Oxygen densities while the loss of plasma increases through charge exchange with molecular species followed by recombination. Poleward meridional winds and westward E-fields can also contribute to plasma loss. It is not uncommon to have less than half the quiet time plasma peak density (NmF2) in an area covered by the composition bulge following a geomagnetic storm. This is what is called the negative ionosphere storm effect. The global neutral composition can take more than 36 hours to recover after a storm.

In the downwelling area the increased atomic Oxygen causes increased plasma production and reduced loss resulting in increased plasma density. This is the positive ionospheric storm. Equatorward meridional winds and eastward E-fields can also contribute to the positive phase.

At a given location, positive storm effects are seen first though not always, followed by negative storm effects (M. V. Codrescu et al., 1992). The ionospheric changes are most pronounced in the F2 layer but can be significant in the whole ionosphere especially during long geomagnetic storms. Meridional winds driven by storms can cross the equator and propagate in the opposite hemisphere.

The system forcing uncertainties are greatly amplified during geomagnetic storms. Small scale electric field variability can increase dramatically, change the spatial distribution of energy input, and more than double the Joule heating that results from the convection average electric fields (M. V. Codrescu et al., 2000). The thermosphere ionosphere coupling and the dynamic changes produced by storms in each of the thermosphere and ionosphere subsystems make the modeling difficult and lead to unacceptably large simulation uncertainties.

2.3 The path forward

There are two ways to mitigate the large forcing uncertainties during storms: measure the forcing, i.e. measure the electric fields and particle precipitation at the necessary grid points every few minutes, or use any available system measurements to estimate an appropriate forcing using a data assimilation scheme. As long as properly measuring the forcing is not possible the only practical solution is a sophisticated data assimilation process, that is, a data assimilation scheme that can take advantage of all available TI measurements to reduce the external forcing uncertainty while also improving model data comparisons.

Developing an assimilation scheme that can take advantage of a variety of TI measurements is a major challenge because the external forcing acts in multiple ways with different time constants and because the system contains feed-back loops with storm-time dependent gains. These complications make the correlations between model variables non-stationary or in other words, state and time dependent. Since the covariance matrix depends on the present state of the system, it has to be calculated or estimated again during each assimilation time step.

One practical way to obtain the covariance is by Monte Carlo estimation methods (Evensen, 2003). An appropriate number of members of the background model (an ensemble) is run with representative forcing variations and statistics of their results are used to estimate a covariance matrix. The accuracy of the estimated covariance is a function of the number of members relative to the number of degrees of freedom of the system, the forcing distribution over the ensemble members, and the error of the system estimation, at the time of the estimation.

3 The Thermosphere Ionosphere Data Assimilation (TIDA) Software

The Thermosphere Ionosphere Data Assimilation (TIDA) software implements an enKF for the TI system. Results from TIDA were first presented in (S. M. Codrescu et al., 2018), although the scheme was not called TIDA at the time. TIDA consists of three parts: the data assimilation code, the background Thermosphere Ionosphere general circulation model CTIPe (M. V. Codrescu et al., 2012), and supporting analysis routines in Python.

CTIPe has a long history going back to the early 1980's (T. J. Fuller-Rowell & Rees, 1980). The model has been running in real time (M. V. Codrescu et al., 2012) for more than ten years and has been tested during both quiet and disturbed conditions (Fedrizzi et al., 2012; M. V. Codrescu et al., 2012; Negrea et al., 2012; Fernandez-Gomez et al., 2019). CTIPe was transitioned into operations at the Space Weather Prediction Center (SWPC) in November 2019. Results from the SWPC real-time operational run are available at: `http://ccmc-swpc.s3-website-us-east-1.amazonaws.com/plots.html`

TIDA uses an ensemble of CTIPe model realizations to obtain a Monte Carlo style approximation of the non-stationary covariance matrix for the TI system. In this paper we will further explore neutral mass density assimilation during the severely disturbed 2003 Halloween storms.

TIDA is unique among data assimilation schemes in targeting strongly forced systems due to its handling of the system forcing. The Kalman state vector is augmented with the external system forcing and consequently the forcing is modified or inferred by the assimilated measurements. This inference allows the scheme to run even in the absence of L1 measurements. The forcing changes resulting from one assimilation time step are used during the following assimilation time step.

In addition to the ensemble members, TIDA also conducts a special member and a reference member. The special member is forced with the best estimate of the external system forcing as inferred in the previous assimilation step. The reference run is forced using the measurements of solar wind from the ACE spacecraft at L1 and F10.7 that would have been available in real-time.

For the results presented here, we have used an ensemble with 75 members. The assimilation time step is 30 minutes and the model time step is one minute. The Kalman state vector, in addition to the augmented forcing parameters discussed above, contains the following fields: neutral temperature, constituent mixing ratios, meridional and zonal neutral winds, and mean molecular mass. The state vector contains over 191 thousand elements while the covariance matrix has over 36 million elements.

TIDA is a research tool that has a very large number of configuration options. Our goal in this paper is to show that the assimilation scheme responds to the measurements and their uncertainty as expected during a significant geomagnetic disturbance and to also highlight that the assimilation scheme is able to use the neutral density measurements to estimate the forcing even in the absence or degradation of L1 measurements. We do not claim that our configuration choices result in the best estimate of the system forcing or the best possible TI simulation for this time period. We plan to tune the scheme and use more diverse measurements to further improve results in the future.

4 Data

The neutral density measurements assimilated in this experiment are derived from very sensitive accelerometers flown on the GRACE-A, GRACE-B, and CHAMP satellites (Sutton, 2011). No bias correction was applied before assimilating the data. Furthermore, the estimated uncertainty provided with the measurements was used directly.

The Advanced Composition Explorer (ACE) satellite monitors the solar wind from the first Lagrange point (L1). Unfortunately, due to a solar energetic particle event, significant portions of the ACE data are bad quality and not usable during the storm period. We have retrieved the available data from the NASA OMNI service (`https://omniweb.gsfc.nasa.gov/form/sc_merge_min1.html`), which provides solar wind values propagated to Earth's magnetopause. During data gaps and outages, the most recent valid solar wind driver value is repeated across the gap.

5 Results

We first discuss results from a run where neutral density measurements from all three satellites, GRACE-A, GRACE-B, and CHAMP, were assimilated. During most assimilation time steps, about 30 measurement/satellite were available for assimilation. Given that fewer than 100 measurements were assimilated in each 30 minute assimilation time step and that normal input parameters are not available for many hours during this period, the results are surprisingly good for such an extreme space weather event. Later in this paper we'll discuss model measurement comparisons when measurements from only one satellite are assimilated at a time, to demonstrate that this is not a lucky coincidence but a consequence of the strongly forced nature of the TI system and of the large scale coherence of the neutral density features in both the real system and in the CTIPe model. We note that all results presented in this paper are along the orbit of the moving satellites and are not orbit averaged.

Figure 1 is a scatter plot of model versus measurement results over the Halloween storms (October 27 - 31, 2003). The left column labeled "Reference" illustrates the CTIPe model results without data assimilation. This is what would have been produced by a CTIPe real-time operational run. The middle column shows "Forecast" model results from TIDA before the present assimilation time step measurements are assimilated, while the right column shows the final "Analysis" TIDA neutral density results. The rows are for the three satellite measurements used in this run: CHAMP (top row), GRACE-A (middle row), and GRACE-B (bottom row). Forecast results can be thought of as assimilation results when only measurements older than 30 minutes are available while analysis means that measurements up to the simulation time are available.

p2/figures/scatter1.pdf

Figure 1. Scatter plot of model vs measurement when three satellite data sets are assimilated. Left column reference state (no assimilation), middle column forecast state, right column analysis state, over the 5 day Halloween 2003 storm period with all 3 satellite data sets assimilated.

The large overestimation of neutral density in the reference run (left column) is caused by the loss of forcing measurements during October 30. The L1 measurements needed for the convection and particle precipitation patterns were compromised by an ongoing solar energetic proton event. Since the operational run must produce results even in the absence of input measurements, the model reuses the last available forcing measurements again and again until new forcing measurements become available. The last available L1 measurements for October 30 were such that they caused a large overestimation of the Joule heating in the model, when repeated, resulting in much larger modeled neutral density for corresponding measurements.

Figure 2 illustrates the forcing parameters for the sub-period 29 - 30 October, 2003. Both the reference forcing (blue) and TIDA forcing (yellow) are shown. The large magnitude of B in the YZ plane and the favorable angle together with the large solar wind velocity result in the large overestimation of Joule heating. The TIDA forcing parameters were inferred by the assimilation scheme from the neutral density measurements.

Neutral density measurements alone do not assure a unique solution for model forcing. The inferred forcing parameters presented in Figure 2 are a best estimate for the model forcing given the distribution of assimilated measurements and their uncertainties and the physics captured in the CTIPe model.

Changes in neutral density at the height of a satellite can result from a change in temperature, a change in neutral composition, or a combination of both. Neutral density measurements alone do not contain enough information to allow TIDA to uniquely determine the cause of a model data discrepancy and properly correct for it during each assimilation time step. This and the continuous change in the position of the satellite measurements over the globe result in the ruggedness of the inferred system forcing. Additional measurements of temperature and/or neutral composition are expected to reduce the variability of the inferred forcing and further improve model data comparisons for neutral density.

Figure 3 shows the measured (yellow), reference (red), forecast (blue), and analysis (black) neutral density values for October 29 and 30, 2003. The overestimation of density by the reference run is again obvious on October 30. On the other hand, at times TIDA slightly underestimates the neutral density. This is most obvious for CHAMP at the end of October 30. We do not have a good explanation for this effect and plan to investigate it further. We suspect the effect to be due to the arbitrary limits we imposed on how much the forcing elements are allowed to change from one assimilation time step to the next with a possible contribution from the non-optimal global coverage of the assimilation data sets.

Scatter plots like Figure 1 for the three single satellite assimilation cases are very similar, show only a little more spread than the 3 satellite assimilation case, are not discussed here but can be seen in Appendix A. The difference in forcing parameters inferred by TIDA for the four assimilation cases are minor, do not bring any revelations, and again are not presented here. The difference in TIDA results when assimilating all data sets at once or one at a time can best be seen in Table 1.

Table 1 summarizes the assimilation results over the 5 day period. The results of the wrong inputs forced upon the reference run by the absence of L1 measurements due to the proton event contamination is obvious and totally unacceptable for an operational run. Using previous neutral density measurements, i.e. measurements made before the present 30 minute assimilation time step, TIDA can infer better system forcing parameters and reduce the along the orbit RMSD from over 140% (CHAMP Reference) to below 21% (CHAMP Forecast) and from over 203% (GRACE-A and B Reference) to less than 26% (GRACE-A and B Forecast). The assimilation of the measurements during p2/figures/plot-forcings1.pdf

Figure 2. Forcing measured or assumed for the reference run (blue) and inferred by TIDA from neutral density measurements alone (yellow).

p2/figures/plot-density1.pdf

Figure 3. Neutral density observed (yellow), reference (red), forecast (blue) and analysis (black) for the three satellites during October 29 and 30, 2003

the assimilation time step further reduces the RMSD to less than 16.5% for CHAMP and to less than 15% for GRACE-A and B.

It is obvious from Table 1 that the best TIDA neutral density results are obtained when all 3 satellite data sets are assimilated at the same time. The fact that the TIDA results are better for any satellite when assimilating all measurements than when assimilating only a particular satellite is evidence that the data sets are consistent with each other, have only small biases relative to each other, and that the model approximates the physics of the system well enough to be able to improve the results far away from the location of any given measurement.

6 Conclusions

We have developed TIDA, an enKF data assimilation software package adapted for strongly externally-forced systems. The strongly forced system requires the estimation of the system forcing parameters at each assimilation time step. This is because the forcing uncertainties are the largest source of uncertainty for model results. In addition, the non-stationary nature of the system encourages the estimation of the covariance matrix during each assimilation time step.

Including the external system forcing parameters in the Kalman state of TIDA allows their estimation based on all system measurements and results in considerable improvement in modeling results. Given enough system measurements, the forcing parameters can be inferred even in the absence of the regular forcing measurements (L1 solar wind and F10.7 values). This can assure uninterrupted modeling operations even when model inputs are not available.

TIDA, the implementation of the enKF used in this study, demonstrates the considerable improvement potential of data assimilation for the TI system modeling. A small number of measurements, fewer than 100 neutral density values assimilated during each 30 minute assimilation time steps over 5 days, can reduce the model data RMSD along the orbit be factors of 7 to 10 vs the reference with bad forcing. Furthermore, we have demonstrated that assimilation of the neutral density from a single satellite improves the specification globally.

The TIDA results further indicate that the estimation of the neutral density covariance matrix with a 75 member ensemble of CTIPe runs is good enough to eliminate the need for covariance localization. This is essential, given the sparse data coverage of neutral density available today.

Appendix A Individual satellite scatter plots

Acknowledgments

The CTIPe model code is open source. A GitHub Docker version of CTIPe is available upon request. Please email Mihail Codrescu (Mihail.Codrescu@noaa.gov) if interested. The TIDA code is commercially available from Vector Space, LLC. Please Email Stefan Codrescu (ssmmcc1@gmail.com) if interested. The CHAMP and GRACE-A and B neutral density measurements were provided by Eric Sutton and are available at: `https://drive.google.com/drive/folders/1oki9WOe3J4U3Pn3yebNaO1a3v-Om5Aho`. The ACE measurements used in this study are from the NASA OMNI service `https://omniweb.gsfc.nasa.gov/form/sc_merge_min1.html`

References

Bilitza, D. (2018, September). IRI the International Standard for the Ionosphere. In

Table 1. Root Mean Square % difference for Reference, Forecast, and Analysis over the 5 day Halloween 2003 storm period.

		All sats		Only CHAMP		Only GRACE-A		Only GRACE-B	
Satellite	Reference	Forecast	Analysis	Forecast	Analysis	Forecast	Analysis	Forecast	Analysis
CHAMP	140.25	20.67	16.37	21.82	18.06	21.87	20.37	21.90	20.24
GRACE A	205.68	25.72	14.97	25.83	24.15	26.55	18.83	26.63	18.88
GRACE B	203.71	25.61	14.98	25.65	23.95	26.50	18.93	26.48	18.85

p2/figures/scatter2.pdf

Figure A1. Scatter plot of model vs measurement when only the CHAMP satellite data set is assimilated. Left column reference state (no assimilation), middle column forecast state, right column analysis state, over the 5 day Halloween 2003 storm period.

p2/figures/scatter3.pdf

Figure A2. Scatter plot of model vs measurement when only the GRACE-A satellite data set is assimilated. Left column reference state (no assimilation), middle column forecast state, right column analysis state, over the 5 day Halloween 2003 storm period.

p2/figures/scatter4.pdf

Figure A3. Scatter plot of model vs measurement when only the GRACE-B satellite data set is assimilated. Left column reference state (no assimilation), middle column forecast state, right column analysis state, over the 5 day Halloween 2003 storm period.

Advances in Radio Science (Vol. 16, pp. 1–11). Copernicus GmbH. Retrieved 2020-12-30, from https://ars.copernicus.org/articles/16/1/2018/ (ISSN: 1684-9965) doi: https://doi.org/10.5194/ars-16-1-2018

Borries, C., Berdermann, J., Jakowski, N., & Wilken, V. (2015). Ionospheric stormsA challenge for empirical forecast of the total electron content. *Journal of Geophysical Research: Space Physics*, *120*(4), 3175–3186. Retrieved 2020-12-30, from https://agupubs.onlinelibrary.wiley.com/doi/abs/10.1002/2015JA020988 (_eprint: https://agupubs.onlinelibrary.wiley.com/doi/pdf/10.1002/2015JA020988) doi: https://doi.org/10.1002/2015JA020988

Burns, A. G., Killeen, T. L., Deng, W., Carignan, G. R., & Roble, R. G. (1995). Geomagnetic storm effects in the low- to middle-latitude upper thermosphere. *Journal of Geophysical Research: Space Physics*, *100*(A8), 14673–14691. Retrieved 2021-01-01, from https://agupubs.onlinelibrary.wiley.com/doi/abs/10.1029/94JA03232 (_eprint: https://agupubs.onlinelibrary.wiley.com/doi/pdf/10.1029/94JA03232) doi: https://doi.org/10.1029/94JA03232

Chartier, A. T., Jackson, D. R., & Mitchell, C. N. (2013). A comparison of the effects of initializing different thermosphere-ionosphere model fields on storm time plasma density forecasts. *Journal of Geophysical Research: Space Physics*, *118*(11), 7329–7337. Retrieved 2020-12-30, from https://agupubs.onlinelibrary.wiley.com/doi/abs/10.1002/2013JA019034 (_eprint: https://agupubs.onlinelibrary.wiley.com/doi/pdf/10.1002/2013JA019034) doi: https://doi.org/10.1002/2013JA019034

Chartier, A. T., Matsuo, T., Anderson, J. L., Collins, N., Hoar, T. J., Lu, G., … Bust, G. S. (2016, January). Ionospheric data assimilation and forecasting during storms. *Journal of Geophysical Research: Space Physics*, *121*(1), 2014JA020799. Retrieved 2017-05-10, from http://onlinelibrary.wiley.com/doi/10.1002/2014JA020799/abstract (Number: 1) doi: 10.1002/2014JA020799

Codrescu, M. V., Fuller-Rowell, T. J., & Minter, C. F. (2004, November). An ensemble-type Kalman filter for neutral thermospheric composition during geomagnetic storms. *Space Weather*, *2*(11), S11003. Retrieved 2017-05-10, from http://onlinelibrary.wiley.com/doi/10.1029/2004SW000088/abstract (Number: 11) doi: 10.1029/2004SW000088

Codrescu, M. V., Fuller-Rowell, T. J., Munteanu, V., Minter, C. F., & Millward, G. H. (2008, September). Validation of the Coupled Thermosphere Ionosphere Plasmasphere Electrodynamics model: CTIPE-Mass Spectrometer Incoherent Scatter temperature comparison. *Space Weather*, *6*(9), S09005. Retrieved 2017-07-31, from http://onlinelibrary.wiley.com/doi/10.1029/2007SW000364/abstract (Number: 9) doi: 10.1029/2007SW000364

Codrescu, M. V., FullerRowell, T. J., Foster, J. C., Holt, J. M., & Cariglia, S. J. (2000). Electric field variability associated with the Millstone Hill electric field model. *Journal of Geophysical Research: Space Physics*, *105*(A3), 5265–5273. Retrieved 2020-12-30, from https://agupubs.onlinelibrary.wiley.com/doi/abs/10.1029/1999JA900463 (_eprint: https://agupubs.onlinelibrary.wiley.com/doi/pdf/10.1029/1999JA900463) doi: https://doi.org/10.1029/1999JA900463

Codrescu, M. V., Negrea, C., Fedrizzi, M., Fuller-Rowell, T. J., Dobin, A., Jakowsky, N., … Maruyama, N. (2012, February). A real-time run of the Coupled Thermosphere Ionosphere Plasmasphere Electrodynamics (CTIPe) model. *Space Weather*, *10*(2), S02001. Retrieved 2017-07-31, from http://onlinelibrary.wiley.com/doi/10.1029/2011SW000736/abstract (Number: 2) doi: 10.1029/2011SW000736

Codrescu, M. V., Roble, R. G., & Forbes, J. M. (1992). Interactive ionosphere modeling: A comparison between TIGCM and ionosonde data. *Journal of Geophysical Research: Space Physics*, *97*(A6), 8591–8600. Retrieved 2020-12-31, from https://agupubs.onlinelibrary.wiley.com/doi/abs/10.1029/91JA02807 (_eprint: https://agupubs.onlinelibrary.wiley.com/doi/pdf/10.1029/91JA02807) doi: https://doi.org/10.1029/91JA02807

Codrescu, S. M., Codrescu, M. V., & Fedrizzi, M. (2018). An Ensemble Kalman Filter for the Thermosphere-Ionosphere. *Space Weather*, *16*(1), 57–68. Retrieved 2020-12-30, from https://agupubs.pericles-prod.literatumonline.com/doi/abs/10.1002/2017SW001752 (_eprint: https://agupubs.onlinelibrary.wiley.com/doi/pdf/10.1002/2017SW001752) doi: https://doi.org/10.1002/2017SW001752

Evensen, G. (1994, May). Sequential data assimilation with a nonlinear quasi-geostrophic model using Monte Carlo methods to forecast error statistics. *Journal of Geophysical Research: Oceans*, *99*(C5), 10143–10162. Retrieved 2016-11-04, from http://onlinelibrary.wiley.com/doi/10.1029/94JC00572/abstract (Number: C5) doi: 10.1029/94JC00572

Evensen, G. (2003, November). The Ensemble Kalman Filter: theoretical formulation and practical implementation. *Ocean Dynamics*, *53*(4), 343–367. Retrieved 2020-12-30, from https://doi.org/10.1007/s10236-003-0036-9 doi: 10.1007/s10236-003-0036-9

Fedrizzi, M., FullerRowell, T. J., & Codrescu, M. V. (2012). Global Joule heating index derived from thermospheric density physics-based modeling and observations. *Space Weather*, *10*(3). Retrieved 2020-12-31, from https://agupubs.onlinelibrary.wiley.com/doi/abs/10.1029/2011SW000724 (_eprint: https://agupubs.onlinelibrary.wiley.com/doi/pdf/10.1029/2011SW000724) doi: https://doi.org/10.1029/2011SW000724

Fernandez-Gomez, I., Fedrizzi, M., Codrescu, M. V., Borries, C., Fillion, M., & Fuller-Rowell, T. J. (2019, November). On the difference between real-time and research simulations with CTIPe. *Advances in Space Research*, *64*(10), 2077–2087. Retrieved 2020-12-31, from http://www.sciencedirect.com/science/article/pii/S0273117719301322 doi: 10.1016/j.asr.2019.02.028

Fuller-Rowell, T., Araujo-Pradere, E., Minter, C., Codrescu, M., Spencer, P., Robertson, D., & Jacobson, A. R. (2006, December). US-TEC: A new data assimilation product from the Space Environment Center characterizing the ionospheric total electron content using real-time GPS data. *Radio Science*, *41*(06), 1–8. (Conference Name: Radio Science) doi: 10.1029/2005RS003393

Fuller-Rowell, T. J., Codrescu, M. V., Roble, R. G., & Richmond, A. D. (1997). How does the thermosphere and ionosphere react to a geomagnetic storm? *Washington DC American Geophysical Union Geophysical Monograph Series*, *98*, 203–225. Retrieved 2020-12-30, from http://adsabs.harvard.edu/abs/1997GMS....98..203F doi: 10.1029/GM098p0203

Fuller-Rowell, T. J., & Evans, D. S. (1987, July). Height-integrated Pedersen and Hall conductivity patterns inferred from the TIROS-NOAA satellite data. *Journal of Geophysical Research: Space Physics*, *92*(A7), 7606–7618. Retrieved 2017-08-04, from http://onlinelibrary.wiley.com/doi/10.1029/JA092iA07p07606/abstract (Number: A7) doi: 10.1029/JA092iA07p07606

Fuller-Rowell, T. J., & Rees, D. (1980, November). A Three-Dimensional Time-Dependent Global Model of the Thermosphere. *Journal of the Atmospheric Sciences*, *37*(11), 2545–2567. Retrieved 2017-08-04, from http://journals.ametsoc.org/doi/abs/10.1175/1520-0469(1980)037%3C2545:ATDTDG%3E2.0.CO;2 (Number: 11) doi: 10.1175/1520-0469(1980)037⟨2545:ATDTDG⟩2.0.CO;2

FullerRowell, T. J., Codrescu, M. V., Moffett, R. J., & Quegan, S. (1994). Response of the thermosphere and ionosphere to geomagnetic storms. *Journal of Geophysical Research: Space Physics*, *99*(A3), 3893–3914. Retrieved 2020-12-30, from https://agupubs.onlinelibrary.wiley.com/doi/abs/10.1029/93JA02015 (_eprint: https://agupubs.onlinelibrary.wiley.com/doi/pdf/10.1029/93JA02015) doi: https://doi.org/10.1029/93JA02015

FullerRowell, T. J., Codrescu, M. V., Rishbeth, H., Moffett, R. J., & Quegan, S. (1996). On the seasonal response of the thermosphere and ionosphere to geomagnetic storms. *Journal of Geophysical Research: Space Physics*, *101*(A2), 2343–2353. Retrieved 2020-12-30, from https://agupubs.onlinelibrary.wiley.com/doi/abs/10.1029/95JA01614 (_eprint: https://agupubs.onlinelibrary.wiley.com/doi/pdf/10.1029/95JA01614) doi: https://doi.org/10.1029/95JA01614

Hedin, A. E., Biondi, M. A., Burnside, R. G., Hernandez, G., Johnson, R. M., Killeen, T. L., … Virdi, T. S. (1991). Revised global model of thermosphere winds using satellite and ground-based observations. *Journal of Geophysical Research: Space Physics*, *96*(A5), 7657–7688. Retrieved 2020-12-31, from https://agupubs.onlinelibrary.wiley.com/doi/abs/10.1029/91JA00251 (_eprint: https://agupubs.onlinelibrary.wiley.com/doi/pdf/10.1029/91JA00251) doi: https://doi.org/10.1029/91JA00251

Heelis, R. A., & Maute, A. (2020). Challenges to Understanding the Earth's Ionosphere and Thermosphere. *Journal of Geophysical Research: Space Physics*, *125*(7), e2019JA027497. Retrieved 2020-12-31, from https://agupubs.onlinelibrary.wiley.com/doi/abs/10.1029/2019JA027497 (_eprint: https://agupubs.onlinelibrary.wiley.com/doi/pdf/10.1029/2019JA027497) doi: https://doi.org/10.1029/2019JA027497

Hinteregger, H. E., Fukui, K., & Gilson, B. R. (1981, November). Observational, reference and model data on solar EUV, from measurements on AE-E. *Geophysical Research Letters*, *8*(11), 1147–1150. Retrieved 2017-10-25, from http://onlinelibrary.wiley.com/doi/10.1029/GL008i011p01147/abstract (Number: 11) doi: 10.1029/GL008i011p01147

Hoar, T., Raeder, K., Anderson, J., Collins, N., Liu, H., Romine, G., … Lawson, G. (2009, December). DART: A Community Facility for Ensemble Data Assimilation. *AGU Fall Meeting Abstracts*.

Hsu, C.-T., Matsuo, T., Wang, W., & Liu, J.-Y. (2014, November). Effects of inferring unobserved thermospheric and ionospheric state variables by using an Ensemble Kalman Filter on global ionospheric specification and forecasting. *Journal of Geophysical Research: Space Physics*, *119*(11), 2014JA020390. Retrieved 2017-05-08, from http://onlinelibrary.wiley.com/doi/10.1002/2014JA020390/abstract (Number: 11) doi: 10.1002/2014JA020390

Jakowski, N., Mayer, C., Hoque, M. M., & Wilken, V. (2011). Total electron content models and their use in ionosphere monitoring. *Radio Science*, *46*(6). Retrieved 2020-12-30, from https://agupubs.onlinelibrary.wiley.com/doi/abs/10.1029/2010RS004620 (_eprint: https://agupubs.onlinelibrary.wiley.com/doi/pdf/10.1029/2010RS004620) doi: https://doi.org/10.1029/2010RS004620

Jee, G., Lee, H.-B., Kim, Y. H., Chung, J.-K., & Cho, J. (2010, October). Assessment of GPS global ionosphere maps (GIM) by comparison between CODE GIM and TOPEX/Jason TEC data: Ionospheric perspective: ASSESSMENT OF GPS GLOBAL IONOSPHERE MAPS. *Journal of Geophysical Research: Space Physics*, *115*(A10), n/a–n/a. Retrieved 2020-12-31, from http://doi.wiley.com/10.1029/2010JA015432 doi: 10.1029/2010JA015432

Killeen, T. L., Burns, A. G., Azeem, I., Cochran, S., & Roble, R. G. (1997, April). A theoretical analysis of the energy budget in the lower thermosphere. *Journal of Atmospheric and Solar-Terrestrial Physics*, *59*(6), 675–689. Retrieved 2020-12-31, from http://www.sciencedirect.com/science/article/pii/S1364682696001149 doi: 10.1016/S1364-6826(96)00114-9

Manoj, C., & Maus, S. (2012, September). A real-time forecast service for the ionospheric equatorial zonal electric field: REAL-TIME ZONAL ELECTRIC FIELD. *Space Weather*, *10*(9), n/a–n/a. Retrieved 2020-12-31, from http://doi.wiley.com/10.1029/2012SW000825 doi: 10.1029/2012SW000825

Mlynczak, M. G., Hunt, L. A., Russell, J. M., Marshall, B. T., Mertens, C. J., & Thompson, R. E. (2016). The global infrared energy budget of the thermosphere from 1947 to 2016 and implications for solar variability. *Geophysical Research Letters*, *43*(23), 11,934–11,940. Retrieved 2020-12-31, from https://agupubs.onlinelibrary.wiley.com/doi/abs/10.1002/2016GL070965 (_eprint: https://agupubs.onlinelibrary.wiley.com/doi/pdf/10.1002/2016GL070965) doi: https://doi.org/10.1002/2016GL070965

Morozov, A. V., Ridley, A. J., Bernstein, D. S., Collins, N., Hoar, T. J., & Anderson, J. L. (2013, November). Data assimilation and driver estimation for the Global Ionosphere-Thermosphere Model using the Ensemble Adjustment Kalman Filter. *Journal of Atmospheric and Solar-Terrestrial Physics*, *104*, 126–136. Retrieved 2017-05-10, from http://www.sciencedirect.com/science/article/pii/S1364682613002289 doi: 10.1016/j.jastp.2013.08.016

Nava, B., Cosson, P., & Radicella, S. M. (2008, December). A new version of the NeQuick ionosphere electron density model. *Journal of Atmospheric and Solar-Terrestrial Physics*, *70*(15), 1856–1862. Retrieved 2021-01-08, from http://www.sciencedirect.com/science/article/pii/S1364682608000357 doi: 10.1016/j.jastp.2008.01.015

Negrea, C., Codrescu, M. V., & FullerRowell, T. J. (2012). On the validation effort of the Coupled Thermosphere Ionosphere Plasmasphere Electrodynamics model. *Space Weather*, *10*(8). Retrieved 2020-12-31, from https://agupubs.onlinelibrary.wiley.com/doi/abs/10.1029/2012SW000818 (_eprint: https://agupubs.onlinelibrary.wiley.com/doi/pdf/10.1029/2012SW000818) doi: https://doi.org/10.1029/2012SW000818

Picone, J. M., Hedin, A. E., Drob, D. P., & Aikin, A. C. (2002). NRLMSISE-00 empirical model of the atmosphere: Statistical comparisons and scientific issues. *Journal of Geophysical Research: Space Physics*, *107*(A12), SIA 15–1–SIA 15–16. Retrieved 2020-12-30, from https://agupubs.onlinelibrary.wiley.com/doi/abs/10.1029/2002JA009430 (_eprint: https://agupubs.onlinelibrary.wiley.com/doi/pdf/10.1029/2002JA009430) doi: https://doi.org/10.1029/2002JA009430

Proelss, G. W., & von Zahn, U. (1978). On the local time variation of atmospheric-ionospheric disturbances. , 159–162. Retrieved 2020-12-31, from http://adsabs.harvard.edu/abs/1978spre.conf..159P (Conference Name: Space Research XVIII)

Richmond, A. D. (1989, September). Modeling the ionosphere wind dynamo: A review. *pure and applied geophysics*, *131*(3), 413–435. Retrieved 2020-12-31, from https://doi.org/10.1007/BF00876837 doi: 10.1007/BF00876837

Roble, R. G. (1992, August). Global dynamic models of the earth's upper atmosphere. , 2313–2328. Retrieved 2020-12-30, from http://adsabs.harvard.edu/abs/1992asdy.conf.2313R (Conference Name: Astrodynamics 1991)

Rockafellar, R. T., & Wets, R. J.-B. (1998). *Variational Analysis*. Berlin Heidelberg: Springer-Verlag. Retrieved 2021-01-07, from https://www.springer.com/gp/book/9783540627722 doi: 10.1007/978-3-642-02431-3

Sarris, T. E. (2019, July). Understanding the ionosphere thermosphere response to solar and magnetospheric drivers: status, challenges and open issues. *Philosophical Transactions of the Royal Society A: Mathematical, Physical and Engineering Sciences*, *377*(2148), 20180101. Retrieved 2020-12-30, from https://royalsocietypublishing.org/doi/10.1098/rsta.2018.0101 (Publisher: Royal Society) doi: 10.1098/rsta.2018.0101

Schunk, R. W., Scherliess, L., Sojka, J. J., Thompson, D. C., Anderson, D. N., Codrescu, M., ... Howe, B. M. (2004). Global Assimilation of Ionospheric Measurements (GAIM). *Radio Science*, *39*(1). Retrieved 2020-12-30, from https://agupubs.onlinelibrary.wiley.com/doi/abs/10.1029/2002RS002794 (_eprint: https://agupubs.onlinelibrary.wiley.com/doi/pdf/10.1029/2002RS002794) doi: https://doi.org/10.1029/2002RS002794

Solomentsev, D. V., Khattatov, B. V., Codrescu, M. V., Titov, A. A., Yudin, V., & Khattatov, V. U. (2012, July). Ionosphere state and parameter estimation using the Ensemble Square Root Filter and the global three-dimensional first-principle model. *Space Weather*, *10*(7), S07004. Retrieved 2017-05-10, from http://onlinelibrary.wiley.com/doi/10.1029/2012SW000777/abstract (Number: 7) doi: 10.1029/2012SW000777

Spencer, P., Robertson, D., & Mader, G. (2004). Ionospheric data assimilation methods for geodetic applications. In *PLANS 2004. Position Location and Navigation Symposium (IEEE Cat. No.04CH37556)* (pp. 510–517). Monterey, CA, USA: IEEE. Retrieved 2020-12-31, from http://ieeexplore.ieee.org/document/1309036/ doi: 10.1109/PLANS.2004.1309036

Sutton, E. (2011). *Accelerometer-Derived Atmospheric Densities from the CHAMP and GRACE Satellites: Version 2.3, AFRL Technical Memo. DTIC# ADA537198.* AFRL Technical Memo. DTIC# ADA537198. Retrieved from https://drive.google.com/drive/folders/1RnnRCPqTJcmsfS13N8ukLF-72k4IfJOL

Weimer, D. R. (2005, May). Improved ionospheric electrodynamic models and application to calculating Joule heating rates. *Journal of Geophysical Research: Space Physics*, *110*(A5), A05306. Retrieved 2017-08-04, from http://onlinelibrary.wiley.com/doi/10.1029/2004JA010884/abstract (Number: A5) doi: 10.1029/2004JA010884

Figure 1.

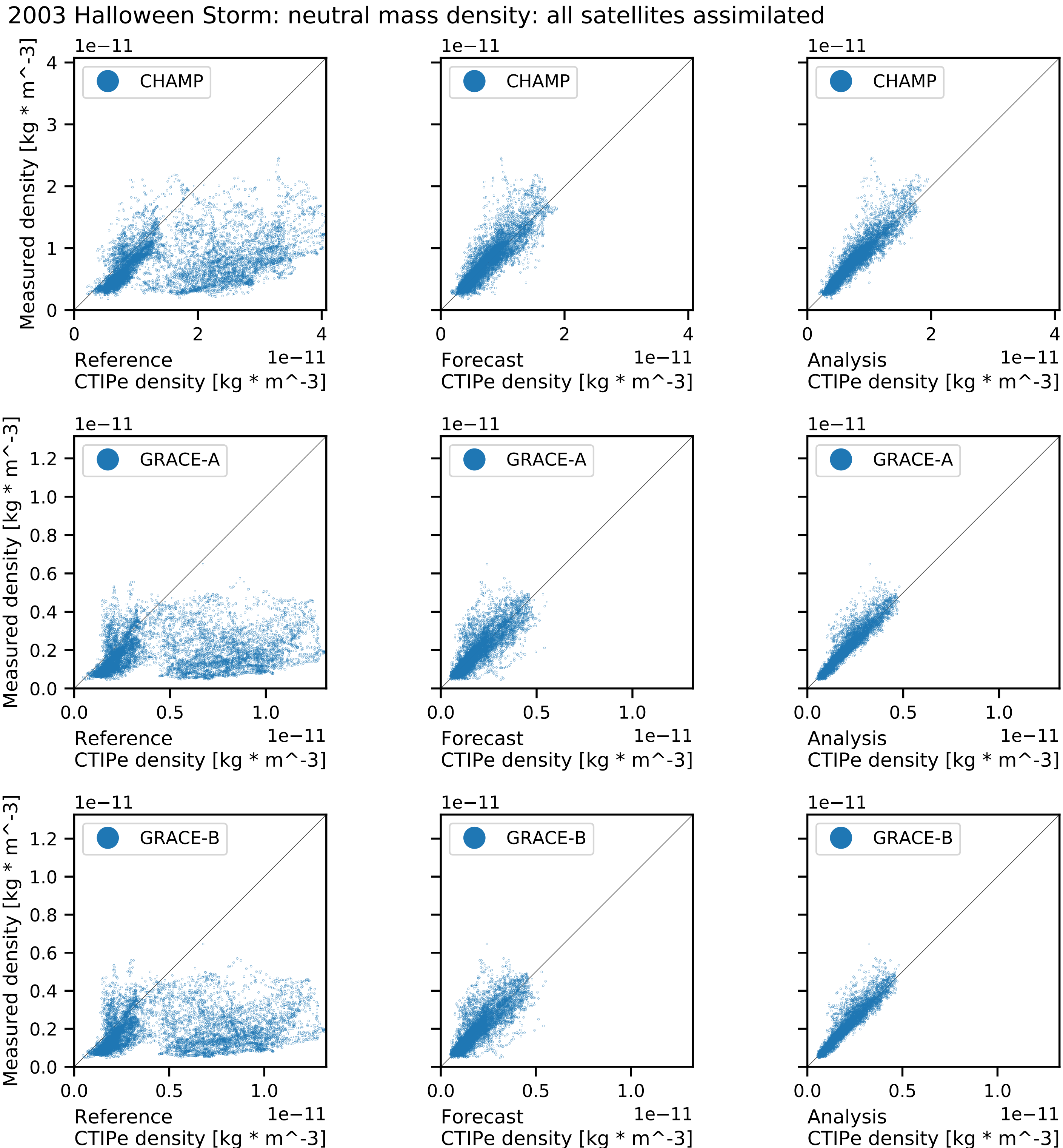

2003 Halloween Storm: neutral mass density: all satellites assimilated
CHAMP
GRACE-A
GRACE-B
Measured density [kg * m^-3]
1e−11
Reference
Forecast
Analysis
CTIPe density [kg * m^-3]

Figure 2.

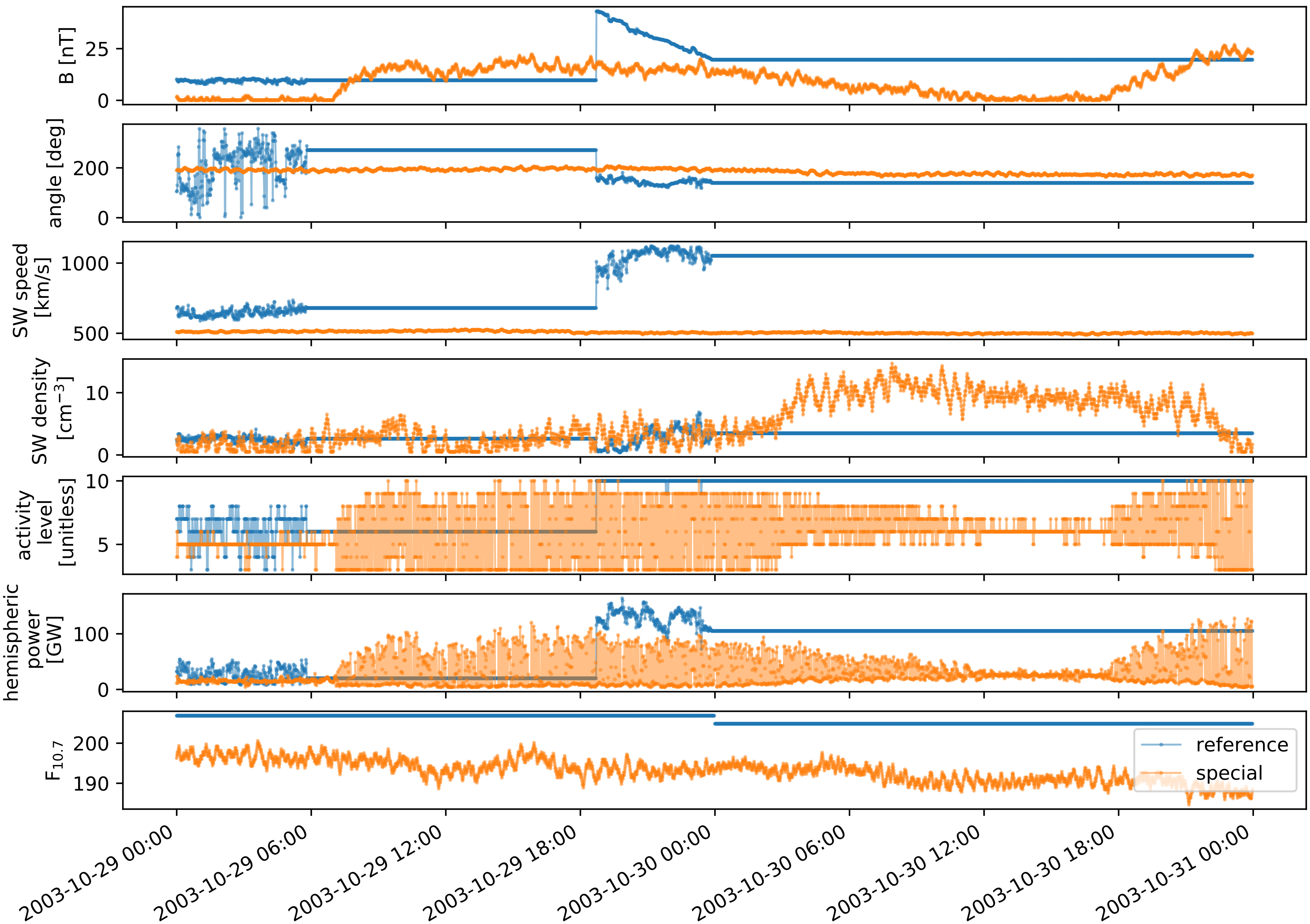

B [nT]
angle [deg]
SW speed [km/s]
SW density [cm^{-3}]
activity level [unitless]
hemispheric power [GW]
$F_{10.7}$
reference
special
2003-10-29 00:00
2003-10-29 06:00
2003-10-29 12:00
2003-10-29 18:00
2003-10-30 00:00
2003-10-30 06:00
2003-10-30 12:00
2003-10-30 18:00
2003-10-31 00:00

Figure 3.

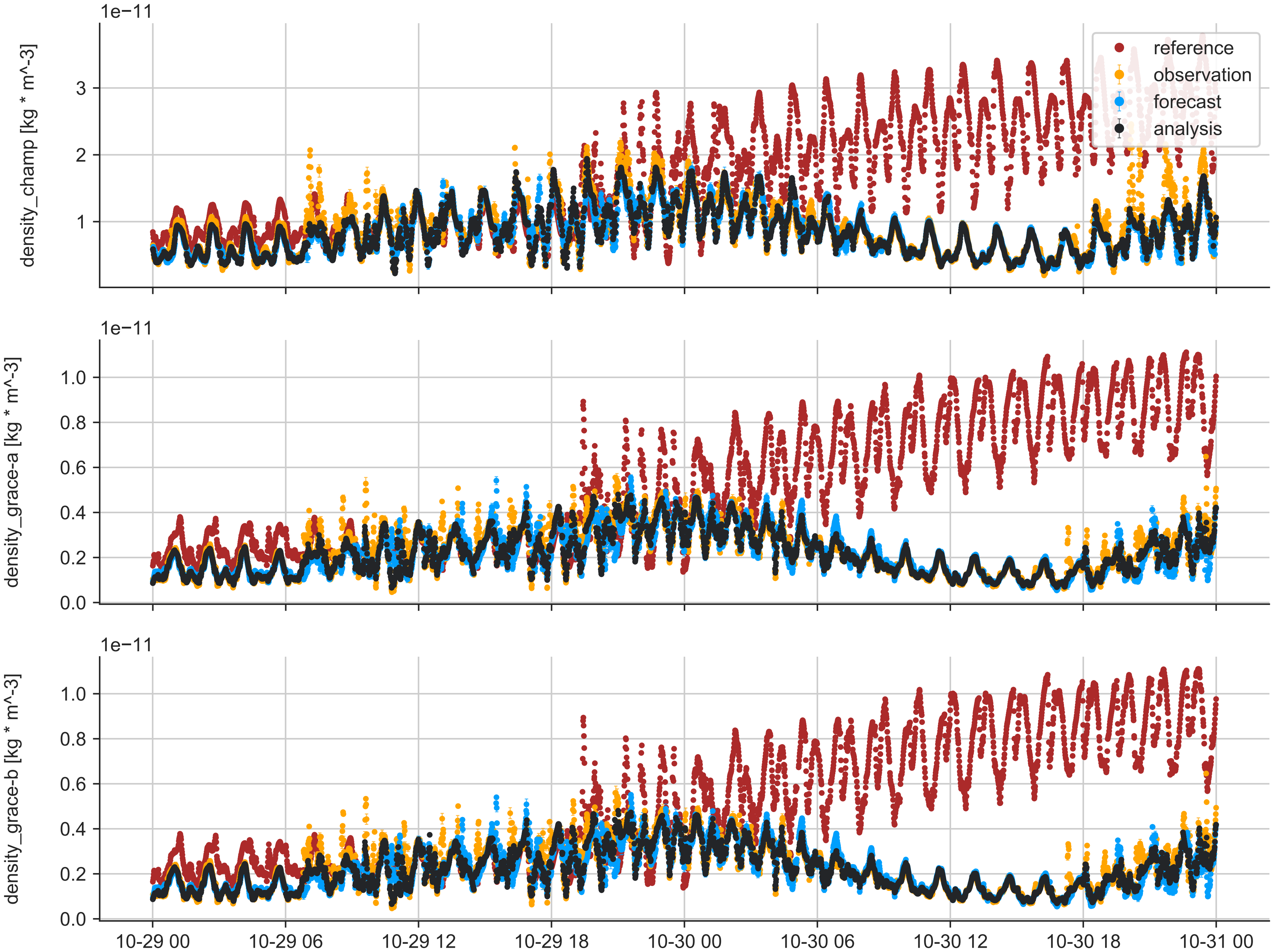

1e−11
density_champ [kg * m^-3]
reference
observation
forecast
analysis
1e−11
density_grace-a [kg * m^-3]
1e−11
density_grace-b [kg * m^-3]
10-29 00
10-29 06
10-29 12
10-29 18
10-30 00
10-30 06
10-30 12
10-30 18
10-31 00

Figure 4.

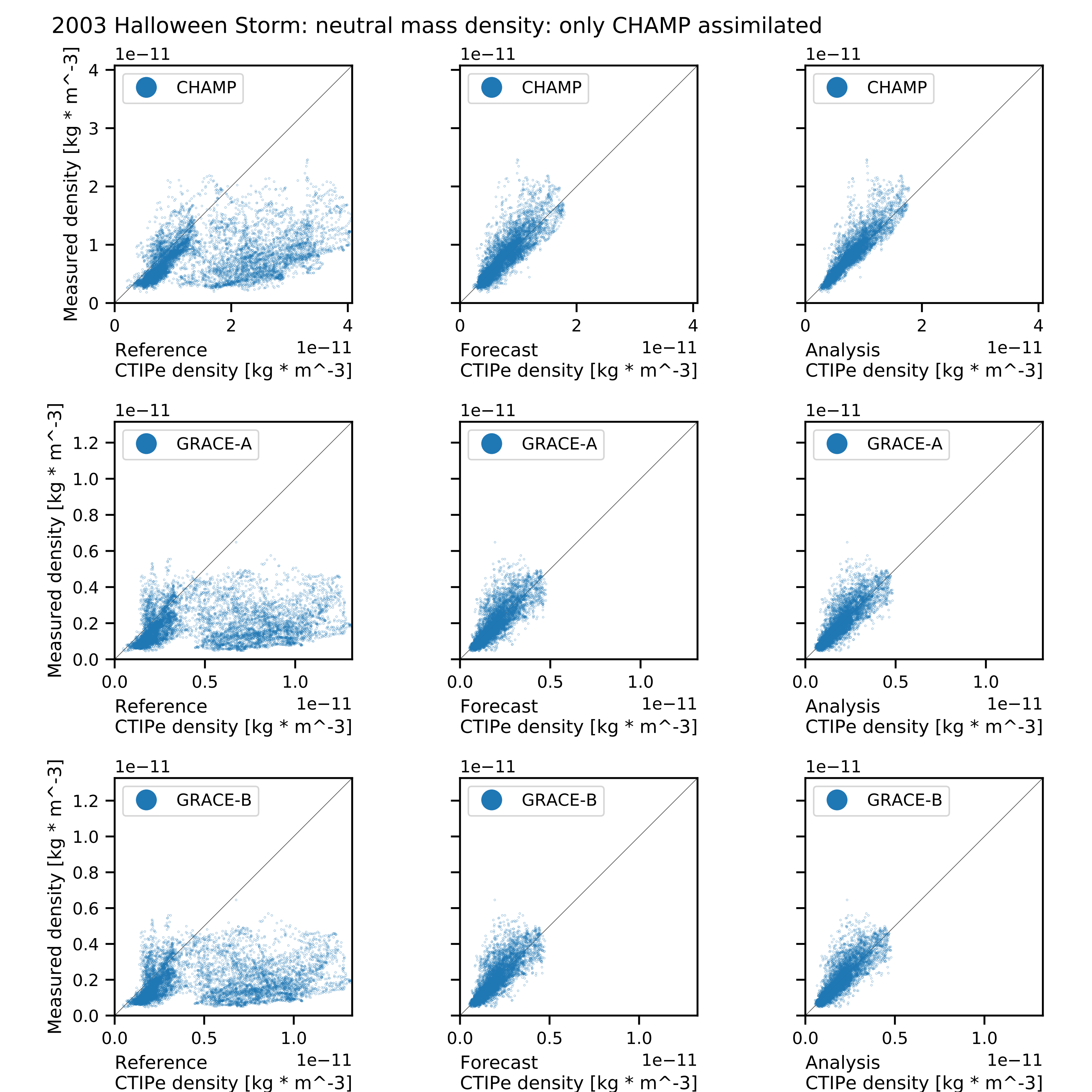

2003 Halloween Storm: neutral mass density: only CHAMP assimilated
CHAMP
GRACE-A
GRACE-B
1e−11
Measured density [kg * m^-3]
Reference
Forecast
Analysis
CTIPe density [kg * m^-3]

Figure 5.

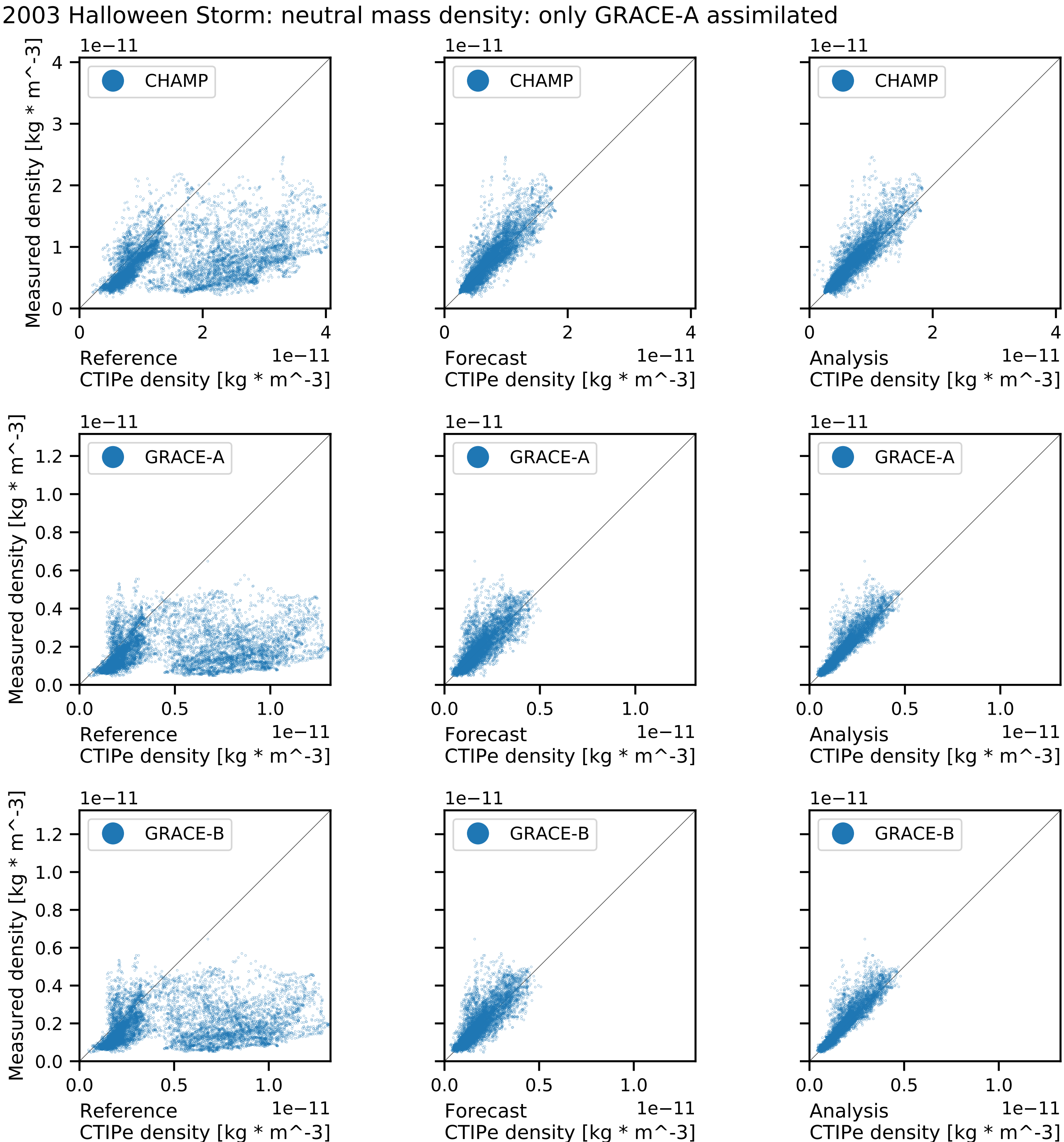
2003 Halloween Storm: neutral mass density: only GRACE-A assimilated
Measured density [kg * m^-3]
1e−11
CHAMP
GRACE-A
GRACE-B
Reference
Forecast
Analysis
CTIPe density [kg * m^-3]

Figure 6.

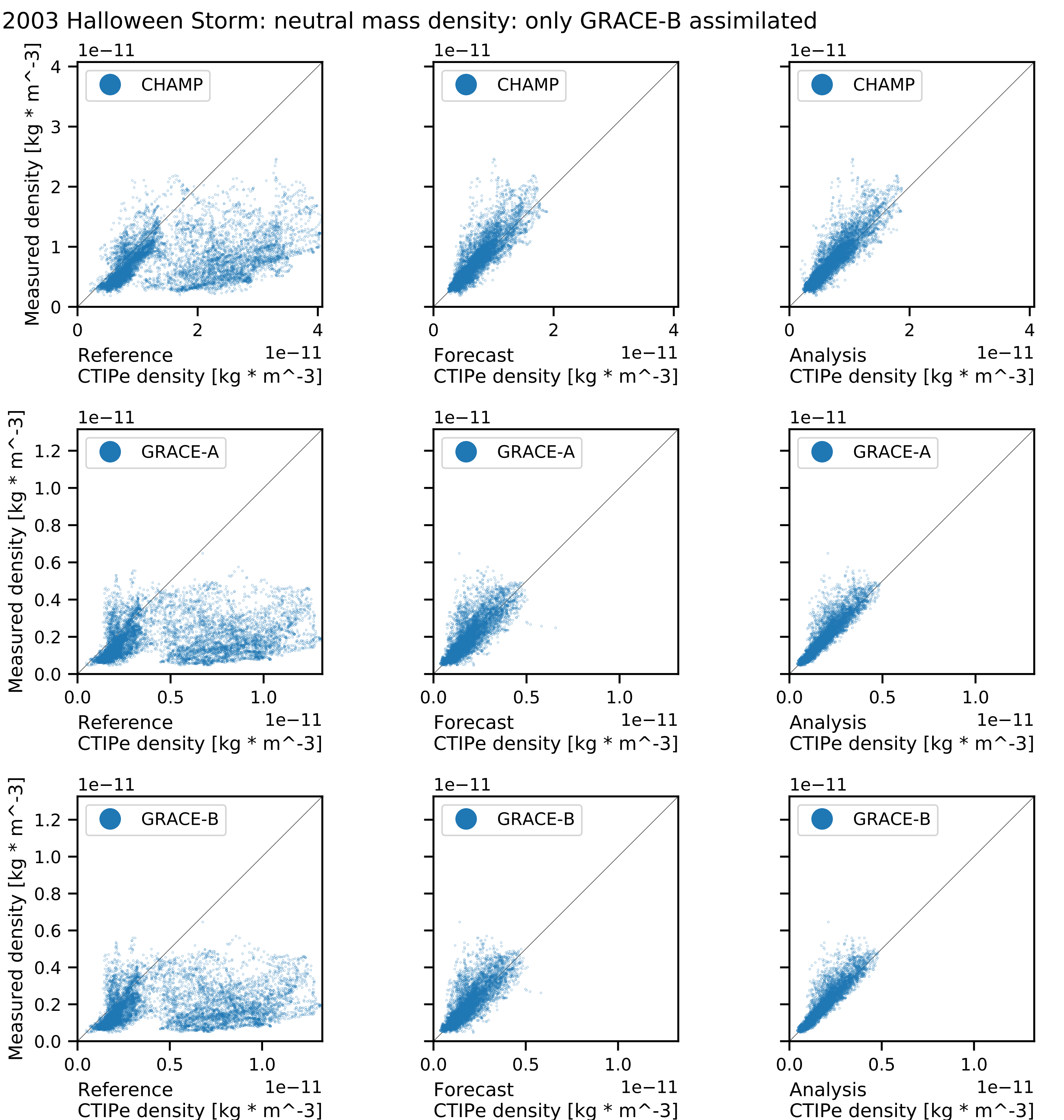

2003 Halloween Storm: neutral mass density: only GRACE-B assimilated
CHAMP
GRACE-A
GRACE-B
Measured density [kg * m^-3]
1e−11
Reference
Forecast
Analysis
CTIPe density [kg * m^-3]